Research Article

Journal of Applied Material Science & Engineering Research

Structure and Correlation Between the Fraction of Structural Units and Bond Angle Distribution in Liquid B_2O_3 Under Compression

Mai Thi Lan* and Nguyen Van Hong

Hanoi University of Science and Technology

***Corresponding author**
Mai Thi Lan, Hanoi University of Science and Technology, Vietnam, E-mail: lan.maithi@hust.edu.vn

Submitted: 15 Mar 2018; **Accepted**: 22 Mar 2018; **Published**: 09 Apr 2018

Abstract

Structure of network-forming liquid B_2O_3 is investigated by Molecular dynamics simulation (MDS) at 2000K and in the 0-40 GPa pressure range (corresponding to the 1.71-3.04 g/cm^3 density range). Results indicate that network structure of liquid B_2O_3 comprises of basic structural units BO_3 and BO_4. The topology and size of BO_3 and BO_4 units at different densities are identical. The O-B-O and B-O-B partial bond angle distributions (BADs) can be determined through the fraction of BO_3 and BO_4 units. Furthermore, the total BADs are directly related to the partial BADs and the fraction of structural units. It means the fraction of units BO_X (X = 3,4) and units OB_y (y = 2,3) can be determined from the experimental BADs. The spatial distribution of BO_3 and BO_4 units is not uniform but forming clusters of BO_3 and BO_4. This leads to the polyamorphism in liquid B_2O_3. It also shows that the dynamical heterogeneity in liquid B_2O_3 due to the lifetimes of BO_3 and BO_4 units are very different. The structural heterogeneity is origin of spatially heterogeneous dynamics in liquids B_2O_3.

Keywords: Boric oxide B_2O_3, Molecular Dynamics Simulation, Network Structure, Polyamorphism, Heterogeneous Dynamics.

Introduction

Boron oxide (B_2O_3) is one of the simplest glass-forming oxides and it is also one of the most important materials with many high-technology applications. Due to its important applications in optical materials and glass ceramics, borate glasses and melts have been investigated by both experiment and computer simulation. The experimental results of Lee, et al. indicate a change coordination number of B-O pair from 3 to 3.46 as pressure increases from 4.1 to 7.3 GPa and increase up to 3.92 at 22.5 GPa [1]. Structural study of B_2O_3 glass by X-ray diffraction was carried out by Warren and he showed that network structure of B_2O_3 consists of BO_3 units which link to each other via bridging oxygen [2]. The boron atoms in the structure of pure B_2O_3 glass are mostly related to B_3O_6 ring. The B_3O_6 rings will be broken and BO_3 and BO_4 units are formed when Na atoms (modifier atoms) are added [3]. Further, modifier atoms also change the dynamical and physical properties along with structural modifications. Investigation by X-ray diffraction in indicated that the O-B-O, O-O-O and B-O-B BADs in B_2O_3 glass have a main peak located at about 120°, 60° and 120°, respectively [4]. There is small sharp peak at 60° in the B-B-B BAD. This results in the presence of many planar boroxol rings (B_3O_6). However, the fraction of boron atoms in the B_3O_6 boroxol rings still in debate [5-9]. According to neutron diffraction experiment, Philip S Salmon showed that at ambient pressure, the mean bond distance and the mean coordination number of B-O atomistic pair is corresponding to about 1.35 Å and around 3.0. The studies showed that, the structures of crystalline B_2O_3 is built by BO_3 units (at low pressure) and BO_4 units (at high pressure) [10-16]. The transformation from BO_3 units to BO_4 units happens at 6.5 GPa. For B_2O_3 liquid, the local structure unchanged as temperature increase up to melting point (at ambient pressure) [17]. The MDS found that non-bridging oxygen linked to a twofold-coordinated boron [18]. This defect coordination relates to atomic diffusion and results in rearrangement of the covalent bonds. Satoshi Ohmura indicated anomalous diffusion in liquid B_2O_3 by ab initio MDS [19]. Diffusion coefficients of B and O atoms in liquid B_2O_3 increases as pressure increases to 10 GPa. Although B_2O_3 has been investigated for many decades but so far, its structure is still debate and requires more studies. One among interesting directions of recent studies is to clarify network structure, relation between structure and dynamic properties. These issues are very difficult to conduct by experiment and ones usually apply the simulation method. MDS can track trajectories of each atom over whole simulation time. Thus, by using MDS, we can get insight into the network structure and dynamics properties of liquid B_2O_3 under high pressure. MDS in recent works concerning B_2O_3 reveal that a gradual transition from BO_3 unit to BO_4 unit induces the variation of total O–B–O and B–O–B BADs [16-22]. It means that there is a correlation between the total O–B–O, B–O–B BADs and the fraction of structural units. However, as far as we know, the correlation between the total O–B–O, B–O–B BADs and the fraction of structural units in liquid B_2O_3 is not clarified. Besides, the number of studies on the polyamorphism and dynamical heterogeneity in liquid B_2O_3 is very limited. In this work, the structural characteristics, polyamorphism and dynamical heterogeneity in liquid B_2O_3 will clarified. Especially, the correlation between the fraction of structural

units and BADs in liquid B_2O_3 will be discussed in detail.

Calculation method

MDS is carried out for B_2O_3 system containing 3000 atoms at temperatures of 2000 K and in the 0-40 GPa pressure range by using Born-Mayer-Huggins potential. The detail of this potential can be found in Ref. [23]. The MD initial configuration is built by randomly placing 3000 atoms in a simulation box with periodic boundary conditions. This sample is equilibrated at temperature of 6000 K to remove the effect of remembering initial configuration after 2.106 MD steps. Then, the sample is cooled down to the temperature of 2000 K and at ambient pressure. The model M1 will be obtained after being relaxed for a long time in an NPT ensemble (number of atom N, pressure P and temperature T are constant). From model M1, by compressing to different pressures (different densities) and then relaxed for a long time to reach the equilibrium, we will obtain 8 models at different densities from 1.71 to 3.04 g/cm^3. To improve the statistics the measured characteristics such as the coordination number, partial radial distribution function (PRDF) are computed by averaging over 1000 configurations separated by 10 MD steps. To evaluate the coordination number and BAD, we use the cut-off distance is 1.90 Å. Here, the cut-off distance is chosen as the position of the first minimum of PRDF gBO(r). To obtain the dynamics characteristics, the computational models were also relaxed for a long time in the NVE ensemble (number of atom N, Volume V and Energy E are constant). The spatial distribution of units BO_3 and BO_4 is also clarified via visualization technique.

Result and Discussion

Pair radial distribution functions

The density dependence of the PRDF $g_{ij}(r)$ is showed figure 1. In $g_{BO}(r)$, the first peak position locates at about 1.36 Å over all densities and becomes more asymmetric with increasing density. After the first peak, there is a very broad peak appears around 2.96 Å in the model when the density approaches 2.96 g/cm^3. This peak is related to the appearance of ring structure at higher density (figure 2). The $g_{BB}(r)$ and $g_{OO}(r)$ is strongly dependent on density. For $g_{BB}(r)$, the first peak shift to left and the height of peak decreases as density increases. For $g_{OO}(r)$, the location of first peak is unchanged but the height of peak decreases as density increases. The $g_{BB}(r)$ and $g_{OO}(r)$ relates to intermediate-range order (IRO). It means that the IRO structure of liquid B_2O_3 is strongly dependent on density. Detail about of structural characteristics of B_2O_3 is shown in table 1. The simulation results for liquid B_2O_3 show a good agreement with experimental data as well as simulation of other works in peak position [4,10,19].

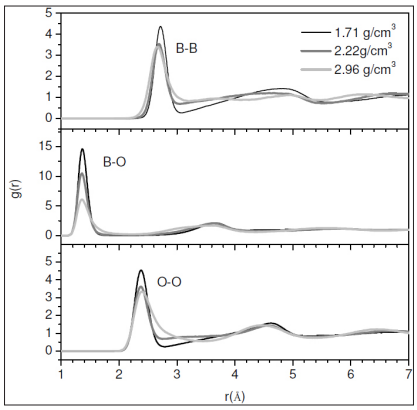

Figure 1: Pair radial distribution functions of liquid B_2O_3 at different densities

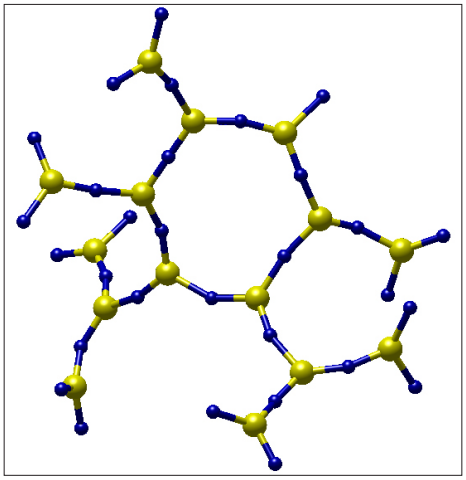

Figure 2: Ring structure in B_2O_3

Table 1: Structural characteristics of liquid B_2O_3. rij - position of first peak of PRDF gij(r); Zij- the mean coordination number; Bx, Oy - the fraction of structural unit BOx and linkage OB_y.

Models	M1	M2	M3	M4	M5	M6	M7	M8	M9	References
r, g/cm^3	1.71	1.90	1.90 2.23	2.44	2.65	2.75	2.87	2.96	3.04	[a]1.69
ZB-O	3.02	3.02	3.06	3.11	3.38	3.47	3.57	3.62	3.69	[b]3.0 [c]3.01
ZO-B	2.01	2.01	2.04	2.08	2.25	2.31	2.38	2.41	2.46	[b]2.0
rB-B, Å	2.72	2.70	2.68	2.66	2.66	2.66	2.66	2.66	2.66	[a]2.7
rB-O, Å	1.36	1.36	1.36	1.36	1.36	1.36	1.36	1.36	1.36	[a]1.4; [c]1.35;
rO-O, Å	2.38	2.36	2.38	2.38	2.40	2.40	2.40	2.40	2.40	[a]2.37
<θO-B-O>	115^0	115^0	110^0	115^0	115^0	110^0	110^0	110^0	110^0	[b][120^0]
<θB-O-O>	160^0	160^0	160^0	155^0	155^0	115^0	115^0	115^0	115^0	[b][120^0]
B^3	0.98	0.98	0.93	0.88	0.62	0.54	0.43	0.39	0.33	
B^4	0.02	0.02	0.07	0.12	0.38	0.46	0.57	0.61	0.67	
O^2	0.99	0.99	0.96	0.92	0.75	0.69	0.63	0.60	0.56	
O^3	0.01	0.01	0.04	0.08	0.25	0.31	0.37	0.40	0.44	

[a,b,c] Experiment and simulation data in [10], [4], [19] respectively.

Distribution of B-O and O-B coordination number

Figure 3 shows the density dependence of fraction of coordination units BOx (x = 3, 4) and
OBy (y=2,3). The results show that at low density (1.71 g/cm^3) the B-O coordination number distribution is characterized by frequencies 3 (98%), 2 (2%) with mean coordination number ZBO= 3.02. The coordination number distribution O-B is characterized by frequencies 2 (99%), 3 (1%) with mean coordination number ZO-B=2.01. It means that at low density, structure of B_2O_3 is built up by units BO_3 and forms continuous random network of the units. The BO_3 basic structural units link each to other via OB_2 linkages at low density. With increasing density, the fraction of units BO_3 monotonously decreases, while the fraction of units BO_4 monotonously increases. At high density (3.04 g.cm-3), the network structure of liquid B_2O_3 comprises of both BO_3 and BO_4 units linked each to other via OB_2 or OB_3 linkages. The B-O coordination number distribution is characterized by frequencies 4 (67%), 3 (33%) with mean coordination number ZB-O=3.69. The coordination number distribution O-B is characterized by frequencies 2 (56%), 3 (44%) with mean coordination number ZO-B=2.46. We can see that there

is a gradual transition from units BO_3 to BO_4 with increasing the density. Note that a transition starts to appear when the density approach 2.80 g/cm^3. The units BOx is connected to each other through common oxygen atoms forming random network structure in three-dimensional space, (figure 4). The simulation results about coordination number as well as bond length, bond angle is also showed a good agreement with experiment and simulation results [4,10,19].

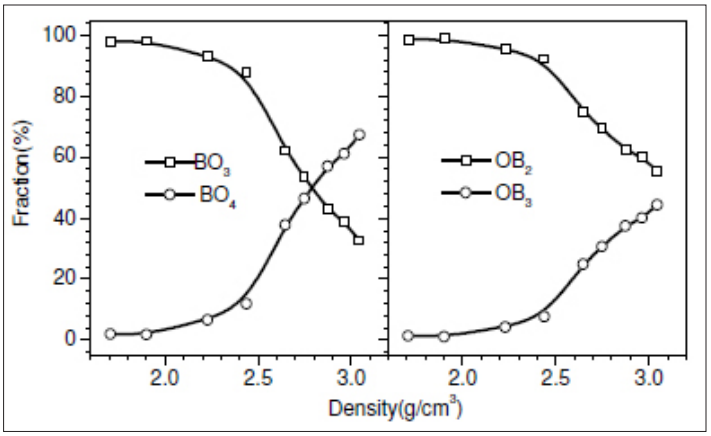

Figure 3: Distribution of B-O and O-B coordination umber as a function of density

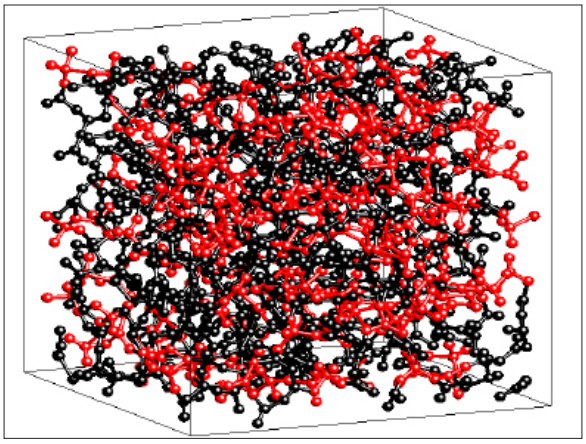

Figure 4: The continuous random network of BO_x units in three-dimensional space at 2.44 g/cm^3, the BO_3 forming region with black color, the BO_4 forming region with red color.

The bond angle and the bond length distributions

To clarify the topology and network structure, the O-B-O and B-O-B bond angle distribution are investigated in detail. The O-B-O bond angle relates to topology of units BOx and B-O-B bond angle relates to the connectivity between the BOx units (network structure). Figure 5 shows partial O-B-O BADs for units BOx (x=3, 4). The results show that the partial O-B-O BAD in BO_3 or BO_4 units is almost the same for different models (different densities). This means that the O-B-O BADs in BO_3 or BO_4 units do not depend on density. The partial B-O-B BADs for coordination units OBy (y=2, 3) is showed in figure 6. The BAD in OB_2 linkages depends strongly on density meanwhile the BAD in OB_3 linkages does not depend on density. The partial B-O BAD in coordination units BO_3, BO_4 is shown in figure 7. For all kinds of coordination units BOx, the B-O bond length decreases with increasing density. The above analysis demonstrates that the bond angle and bond length distribution in BOx units is not dependent of pressure. In other word, the topology structure of BOx units in different models is identical. With increasing density, liquid B_2O_3 gradually transforms from the network structure of BO_3 (at low density) to network structure of BO_4 (at high density). These results are good agreement with experimental data [4].

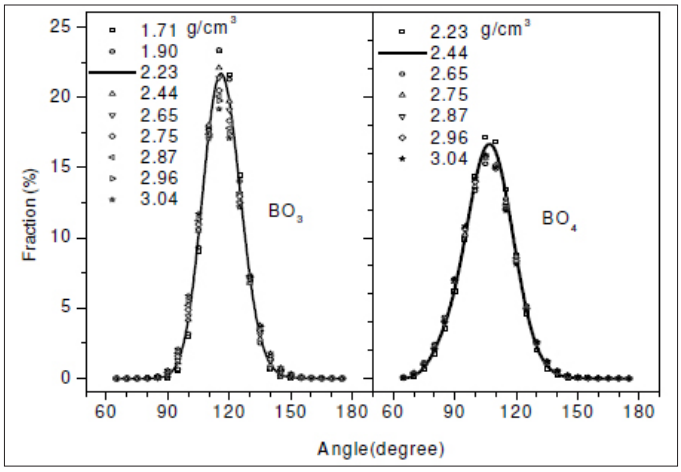

Figure 5: The O-B-O bond angle distribution in BO_3 and BO_4 units

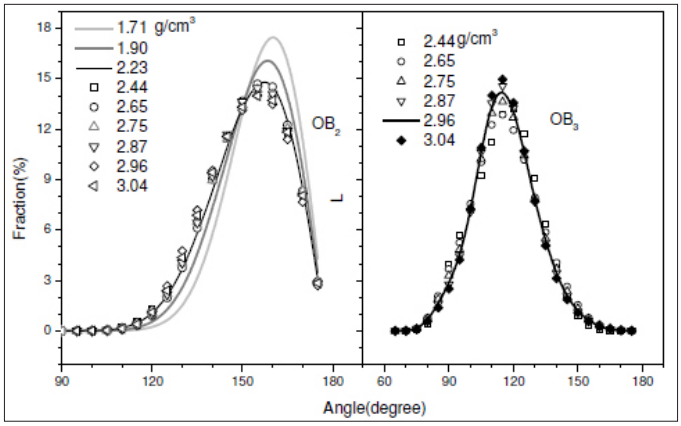

Figure 6: The B-O-B bond angle distribution in OB_2 and OB_3 linkages

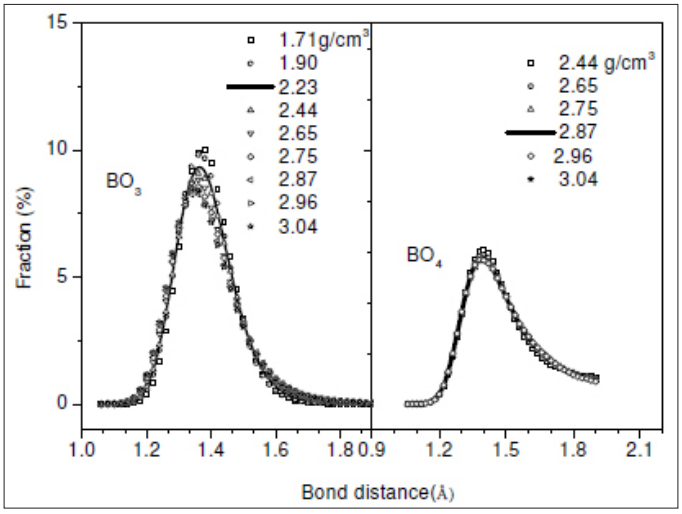

Figure 7: The B-O bond distance distribution in BO_3 and BO_4 units

The correlation between the fraction of structural units and bond angle

We will focus on investigating BADs and establishing the correlation between the fraction of structural units and total BADs. To establish the correlation, let n_{Bx} denote the number of units BO_x (x = 3, 4). The total number of O-B-O angles in BO_3 and BO_4 is 3nB3, 6nB4, respectively. We denote $m_{Bx}(\theta)$ to the number of angles in interval $\theta \pm d\theta$ in units BO_x. The probability that given angle in interval q ± dθ in a sample is given by

$$g_B(\theta) = \frac{m_{B3}(\theta) + m_{B4}(\theta)}{3n_{B3} + 6n_{B4}} = 3Ag_{B4}(\theta)B_3 + 6Ag_{B4}(\theta)B_4 \qquad (1)$$

Here $A = (n_{B3}+n_{B4})/(3n_{B3}+6n_{B4})$; $g_{B3}(\theta)=m_{B3}(\theta)/3n_{B3}$; $g_{B4}(\theta)=m_{B4}(\theta)/6n_{B4}$. The function $g_{Bx}(\theta)$ in fact represents the probability that the given O-B-O angle in units BOx lies in the interval of $\theta \pm d\theta$. Therefore, the function $gB(\theta)$ described the total O-B-O BAD can be expressed via the fraction B_x and functions $g_{Bx}(\theta)$ which represent the partial BAD for units BO_x. Here notation B_x (x =3,4) is the fraction of BO_x in sample. The value of B_x is given in table 1. Because the topology structure of BO_x units in different models is identical so there are the common functions $g_{Bx}(\theta)$ for all considered models. These functions are presented in Figure 5. For both kind of units BO_3 and BO_4, function $g_{B3}(\theta)$ has a form of Gauss function and a pronounced peak at 115o; the case of BO_4, function $g_{B4}(\theta)$ has a peak at 115°. Figure 8 shows the total O-B-O BADs for B_2O_3 models together with the result calculated by equation (1) at different densities. The total O-B-O BAD changes strongly with density. Its main peak slightly shifts to lower angle and the height of main peak decreases with the density. Furthermore, it is clearly that the calculation result is in good agreement with simulation data. It means that we can determine the fraction of units BO_3 and BO_4 from experiment BAD based on known functions $g_{Bx}(\theta)$. By similar way, the total B-O-B BAD can be given as

$$g_O(\theta) = \frac{m_{O2}(\theta) + m_{O3}(\theta)}{n_{O2} + 3n_{O3}} = Bg_{O2}(\theta)O_2 + 3Bg_{O3}(\theta)O_3 \qquad (2)$$

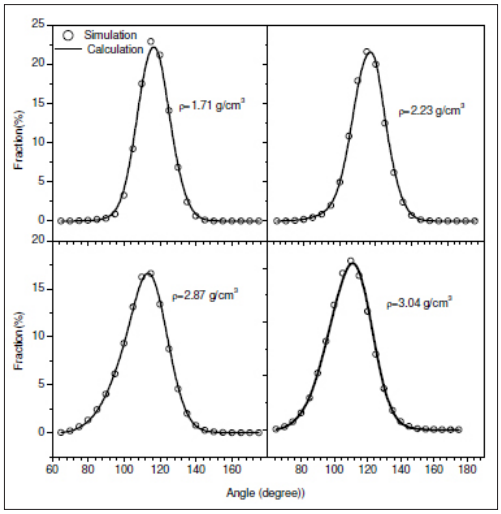

Figure 8: The total O-B-O bond angle distribution; the symbols show simulation data; the lines show data calculated by Equation (1)

where $g_{O2}(\theta)=m_{O2}(\theta)/n_{O2}$;$g_{O3}(\theta)=m_{O3}(\theta)/n_{O3}$; $B=(n_{O2} + n_{O3})/(n_{O2} + 3n_{O3})$. Similar to $g_{Bx}(\theta)$. The function g$Oy(\theta)$ represents the probability that the given B-O-B angle in OB_y lies in the interval of $\theta \pm d\theta$. Here notation O_y (y =2, 3) is the fraction of OB_y in sample. The value of O_y is given in table 1.

The partial bond angle distributions for OB_y are shown in Figure 6 and 9. For OB_2 linkages, $g_{O2}(\theta)$ has a main peak at 160⁰; in the case of OB_3, function $g_{O3}(\theta)$ has peaks at 115°. The total B-O-B BADs are shown in figure 9. It reveals that with increasing the density, the total B-O-B bond angle shifts to the lower angle. The results also reveal that, there is a good agreement between simulation result and data calculated by equation (2).

Structural and dynamical heterogeneities

To clarify the structural and dynamical heterogeneities in liquids B_2O_3, we have visualized the spatial distribution of BO_x and calculated the mean lifetime of the structural units BO_x in B_2O_3 system at different densities. Figure 10 showed that the distribution of coordination units BO_x is not uniform, but they tend to form the cluster of units BO_x. It means that in the considered density range the structure of liquid BO_x comprises two structural phases: BO_3-structural phase (black color), BO_4-structural phase (red color). From figure 9 at low density (1.90 g/cm³) the regions with units BO_3 are linked to each other forming a large region (BO_3-phase) expanding nearly whole model. The regions with units BO_4 (BO_4-phase) are very small and localized at different locations. With increasing density, the regions with BO_4-phase are expanded and the regions with BO_3-phase are shrunk. At 3.04 g/cm³, the regions with BO_4-phase are nearly expanded whole model. The clusters of BO_3 form low density regions, conversely clusters of BO_4 form high density regions. The size of low- and high-density regions is strongly dependent on density (pressure). It means that there is a structural phase transformation from BO_3-structural phase to BO_4-structure with increasing density. Furthermore, in the Figure 11, the lifetime of BO_3 decreases strongly, while the lifetime of BO4 increases. Results show that at low density, the structure of liquids B_2O_3 mainly consist of BO_3 phases and lifetime of units BO_3 is very long in comparison with the one of units BO_4. In contrast, at high density, the structure of above liquid mainly consists of BO_3- and BO_4-phases and the lifetime of time of units BO4 is shorter the one of units BO_3. This means that BO_4-phase will form mobile regions while BO_3-phases will form immobile regions. This leads to the polyamorphism or structural heterogeneity in 5 liquid B_2O_3. Furthermore, the structural heterogeneity in liquids B_2O_3 is origin of spatially heterogeneous dynamics.

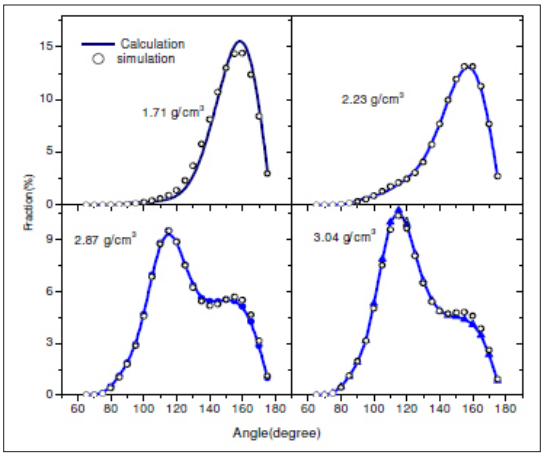

Figure 9: The total B-O-B bond angle distribution; the symbols show simulation data; the lines show data calculated by Equation (2)

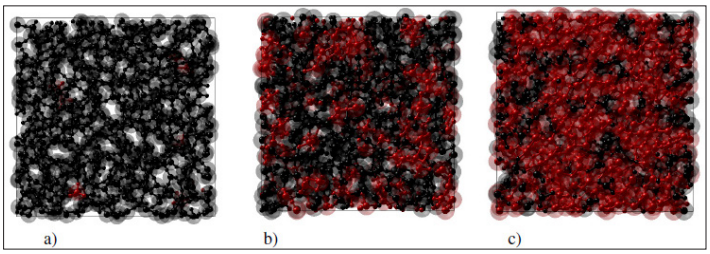

Figure 10: The spatial distribution of units BOx at 1.90 g/cm3 (a); 2.65 g/cm3 and 3.04 g/cm3. The black region is cluster BO3, the red region is cluster BO4. Big sphere is B and small sphere is O atoms.

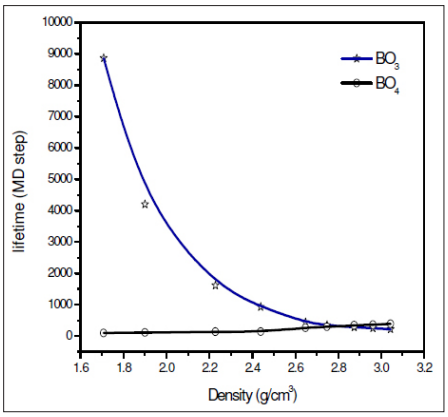

Figure 11: The density dependence of lifetime of coordination units BOx (x = 3,4). Unit lifetime is MD steps.

Conclusion

In this work, MDS methods were applied for investigating the structure and correlation between the fraction of structural units and bond angle distribution of liquid B_2O_3 under compression. Results show that the structure of B_2O_3 comprises basic structural units BO_x (x=3, 4) and OBy (y=2,3) linkages. At low density, most of basic structural units are BO_3. At high density, most of basic structural units are BO_4. Under compression, there is a transformation from BO_3-network structure (at low density) to BO_4-network structure (at high density) in network structure of liquid.

The partial bond angle and bond length distribution in BO_x units is not dependent on density. The topology structure of units BO_x and OBy linkages at different densities is identical. As a result, all models have the same partial BADs $g_{Bx}(\theta)$ and $g_{Oy}(\theta)$. This result allows us to establish a simple correlation between the BADs and the fractions of BO_x units and OB_y linkages. The simulation results show a good agreement with data calculated by obtained expression for both total B-O-B and O-B-O BADs. The distribution of units BO_x is not uniform, but it tends to form clusters of BO_3, BO_4. With increasing density, the size of regions with BO_3-phase decreases and the size of regions with BO_4-phase increases. The BO_4-phase forms mobile regions, while BO_3-phase forms immobile regions. Polyamorphism or structural heterogeneity in liquids $B2O_3$ is the structural origin of spatially heterogeneous dynamics.

Acknowledgement

This work was supported by Hanoi University of Science and Technology - T2017-PC-139.

References

1. Youngman RE (1995) Science 269: 1416.
2. Mozzi RL,Warren BE (1970) J Appl Crystallogr 3: 251.
3. Ahlawat NN, Agamkar P, Ahlawat N, Agarwal A, Monica (2013) Adv Mat Lett 4: 71-73.
4. Suzuya, Yoneda K, Kohara Y, Umesaki S (2000) Phys Chem Glasses Eur J 41: 282-285.
5. Huang L, Kieffer J (2006) Phys Rev B 74: 224107.
6. Swenson J, Borjesson L (1997) Phys Rev B 55: 11138.
7. Hannon AC, Grimley DI, Hulme RA, Wright AC, Sinclair RN (1994) J Non-Cryst Solids 177: 299.
8. Swenson J, Orjesson LB (2006) Phys Rev Lett 96: 199701.
9. Umari P, Pasquarello A (2006) Phys Rev Lett 96: 199702.
10. Philip S Salmon, Anita Zeidler (2015) J Phys Condens Matter 27: 133201.
11. Anita Zeidler, Kamil Wezka, Dean AJ, Whittaker, Philip S Salmon, et al. (2014) Phys Rev B 90: 024206.
12. Gurr GE, Montgomery PW, Knutson CD, Gorres BT (1970) Act Cryst B 26: 906.
13. Johnson PAV, Wright AC, Sinclair RN (1982) J Non-Cryst Solids 50: 281.
14. Prewitt CT, Shannon RD (1968) Act Cryst B 24: 869.
15. Nieto-Sanz D, Loubeyre P, Crichton W, Mezouar M (2004) Phys Rev B 70: 214108.
16. Brazhkin VV, Katayama Y, Trachenko K, Tsiok OB, Lyapin AG, et al. (2008) Phys Rev Lett 101: 035702.
17. Sakowski J, Herms G (2001) J Non-Cryst Solids 2001: 293295.
18. Ohmura S, Shimojo F (2008) Phys Rev B 78: 224206.
19. Satoshi Ahmura, Fuyuki Shimojo (2010) Phys Rev B 81: 014208.
20. Satoshi Ohmura, Fuyuki Shimojo (2012) J Phys Conf Ser 402: 012012.
21. Ohmura S, Shimojo F (2009) Phys Rev B 80: 020202.
22. Ohmura S, Shimojo F (2010) Phys Rev B 81: 014208
23. Verhoef AH, den Hartog HW (1992) J Non-Cryst Solids 146: 267278.